MOLECULAR IMAGING AND BIOLOGY

Mol Imaging Biol (2019) 21:676–685
DOI: 10.1007/s11307-018-1284-x

Published Online: 10 October 2018

RESEARCH ARTICLE

Evaluation of the Novel PET Tracer [^{11}C]HACH242 for Imaging the GluN2B NMDA Receptor in Non-Human Primates

Jasper van der Aart,[1,2] Maqsood Yaqub,[1] Esther J. M. Kooijman,[1] Jaco Bakker,[3] Jan A. M. Langermans,[3] Robert C. Schuit,[1] Mark B. M. Hofman,[1] Johannes A. M. Christiaans,[1] Adriaan A. Lammertsma,[1] Albert D. Windhorst,[1] Bart N. M. van Berckel[1]

[1]*Department of Radiology & Nuclear Medicine, Amsterdam UMC, VU University Medical Center, Amsterdam, The Netherlands*
[2]*Centre for Human Drug Research, Leiden, The Netherlands*
[3]*Animal Science Department, Biomedical Primate Research Centre, Rijswijk, The Netherlands*

Abstract

Purpose: There are currently no positron emission tomography (PET) radiotracers for the GluN2B (NR2B) binding sites of brain *N*-methyl-D-aspartate (NMDA) receptors. In rats, the GluN2B antagonist Ro25-6981 reduced the binding of N-((5-(4-fluoro-2-[^{11}C]methoxyphenyl)pyridin-3-yl)methyl)cyclopentanamin ([^{11}C]HACH242). This paper reports the evaluation of [^{11}C]HACH242 PET in non-human primates at baseline and following administration of the GluN2B negative allosteric modulator radiprodil.

Procedures: Eight 90-min dynamic [^{11}C]HACH242 PET scans were acquired in three male anaesthetised rhesus monkeys, including a retest session of subject 1, at baseline and 10 min after intravenous 10 mg/kg radiprodil. Standardised uptake values (SUV) were calculated for 9 brain regions. Arterial blood samples were taken at six timepoints to characterise pharmacokinetics in blood and plasma. Reliable input functions for kinetic modelling could not be generated due to variability in the whole-blood radioactivity measurements.

Results: [^{11}C]HACH242 entered the brain and displayed fairly uniform uptake. The mean (± standard deviation, SD) T_{max} was 17 ± 7 min in baseline scans and 24 ± 15 min in radiprodil scans. The rate of radioligand metabolism in plasma (primarily to polar metabolites) was high, with mean parent fractions of 26 ± 10 % at 20 min and 8 ± 5 % at 85 min. Radiprodil increased [^{11}C]HACH242 whole-brain SUV in the last PET frame by 25 %, 1 %, 3 and 17 % for subjects 1, 2, 3 and retest of subject 1, respectively. The mean brain to plasma ratio was 5.4 ± 2.6, and increased by 39 to 110 % in the radiprodil condition, partly due to lower parent plasma radioactivity of −11 to −56 %.

Conclusions: The present results show that [^{11}C]HACH242 has a suitable kinetic profile in the brain and low accumulation of lipophilic radiometabolites. Radiprodil did not consistently change [^{11}C]HACH242 brain uptake. These findings may be explained by variations in cerebral blood flow, a low fraction of specifically bound tracer, or interactions with endogenous NMDA receptor

This article replaces Article 1281 –deleted from system. All files from that article included in zip.

Correspondence to: Jasper van der Aart; *e-mail:* jaspervanderaart@gmail.com

ligands at the binding site. Further experiments of ligand interactions are necessary to facilitate the development of radiotracers for *in vivo* imaging of the ionotropic NMDA receptor.

Key words: [11C]HACH242, GluN2B, NMDA, NR2B, PET, Radiprodil

Introduction

N-methyl-D-aspartate (NMDA) receptors are ionotropic glutamate receptors that mediate excitatory postsynaptic signalling and are expressed widely in the central nervous system (CNS). NMDA receptors are heterotetramers of mostly GluN1 and two GluN2(A-D) subunits in the CNS [1]. In the last decade, a major effort in NMDA receptor drug development has focused on allosteric modulation of ion channel activity *via* GluN2B (also known as NR2B) binding sites which are located on the extracellular N-terminal domain (NTD) of the NMDA receptor. Ligands such as ifenprodil and derivatives are noncompetitive antagonists of the GluN2B site that stabilise a closed-cleft conformation of the GluN2B NTD [2]. Immunoblotting techniques showed that in the human brain, the GluN2B subunit is predominantly expressed in the cortex, hippocampus and thalamus, consistent with findings in rats showing high expression in the forebrain. Lower levels of GluN2B are found in the midbrain, cerebellum and spinal cord [3, 4]. The interest in the therapeutic potential of GluN2B negative allosteric modulators has spurred drug development of ifenprodil derivatives in the past two decades. Second generation "prodils" such as radiprodil (RHG-896), traxoprodil (CP-101,606), besonprodil (CI-1041), CERC-301 (MK-0657), EVT-101, Ro 25-6981 and BMT-108908 have been developed for the treatment of a wide range of CNS pathologies, including acute and chronic pain, stroke, dementias and major depressive disorder.

The highest level of confidence and direct evidence that GluN2B engagement is achieved is acquired from *in vivo* molecular imaging experiments with positron emission tomography (PET). There are currently no PET radiotracers available that have shown reliable quantitative specific binding of GluN2B *in vivo*. Radiotracer development for NMDA receptors has been unsuccessful due to suboptimal physiochemical and pharmacological characteristics of ligands such as affinity, lipophilicity, stability, blood-brain barrier penetration and pharmacokinetics [5–10]. Based on the discovery of a new class of GluN2B antagonists [11], N-((5-(4-fluoro-2-[11C]methoxyphenyl)pyridin-3-yl)methyl) cyclopentanamine was synthesised and radiolabelled with carbon-11 ([11C]HACH242, Fig. 1) for preclinical evaluation. Biodistribution and blocking studies with [11C]HACH242 were carried out in anaesthetised mice and in non-anaesthetised rats [12]. The affinity of [11C]HACH242 for GluN2B receptors was 12.4 ± 2.1 nM as shown in competition binding experiments against 5 nM [3H]ifenprodil, which is equal to ifenprodil and about 5 times lower than Ro25-6981. Brain distribution studies in mice showed a threefold increase in activity uptake in forebrain regions *vs.* cerebellum at 15 min, which is the highest ratio that has been reported for candidate GluN2B site radiotracers. [11C]HACH242 binding in non-anaesthetised rats was reduced by Ro25-6981, showing a regional distribution that is consistent both with the expression pattern of GluN2B subunits and the density of [3H]Ro25-6981 binding sites in the adult rodent brain. However, high levels of non-specific uptake were observed in the thalamus [12].

GluN2B ligands frequently exert off-target effects. For example ifenprodil dose-dependently reduces brain uptake of the sigma-1 receptor radiotracer [11C]SA4503 [13]. The selectivity of [11C]HACH242 for GluN2B was investigated in an exhaustive pharmacological screen against 79 targets [12]. The radioligand showed affinity > 1.1 μM for 78 of the targets. Sigma-1 was the exception, for which the tracer showed an affinity of 20 nM. Further studies with GluN2B specific antagonists are warranted to investigate the specific binding of [11C]HACH242 *in vivo*. Radiprodil binds to GluN2B-containing receptors irrespective of the GluN2 subunit composition, analogous to Ro25-6981 [14]. Furthermore, radiprodil binding is insensitive to 1,3-di-o-tolylguanidine (DTG), which suggests it does not bind to the sigma receptors [14]. Research on non-human primates (NHP) generates complementary data that can bridge translational imaging research from rodents to humans. This paper reports on the initial assessment of [11C]HACH242 PET in NHP at baseline and following intravenous administration of a high dose of radiprodil.

Materials and Methods

Animals, Housing and Care

Three adult male rhesus monkeys (*Macaca mulatta*) were selected for this study. Subject and radiotracer injectate details are shown in Table 1. All animals originated from and were housed at the Biomedical Primate Research Centre (BPRC, Rijswijk, The Netherlands), and underwent a complete physical, haematological, and biochemical examination before the study started. They remained under intensive veterinary supervision during the entire study period. Animals were housed in enriched cages at a temperature between 20 and 22 °C, with a 12-h light/12-h dark cycle per day. Drinking water was provided *ad libitum* but food was withheld for 16 h prior to anaesthesia. Ethics approval by the Animal Experiments Committee (DEC) of

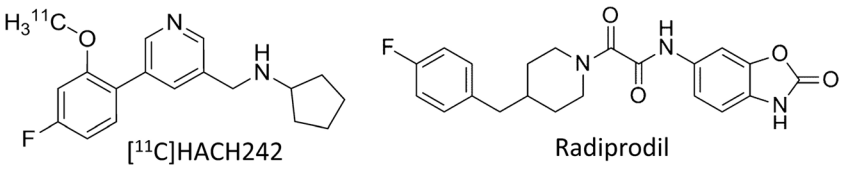

Fig. 1. Chemical structures of [11C]HACH242 and radiprodil.

the BPRC was obtained prior to the commencement of the study. The procedures performed in this study were in accordance with the Dutch laws on animal experimentation, with the regulations for animal handling as described in the EU Directive 63/2010 and with the Weatherall report [15]. The BPRC is accredited by the Association for Assessment and Accreditation of Laboratory Animal Care International.

Study Design, Anaesthesia and Treatment

Three subjects underwent PET and magnetic resonance imaging (MRI) scans on an Philips Ingenuity Time-of-Flight PET/MRI scanner at the Department of Radiology & Nuclear Medicine of the VU University Medical Center (Amsterdam, the Netherlands). Each subject was scanned twice on the same day at baseline and 10 min after radiprodil IV administration. Subject 1 completed a second baseline and radiprodil PET scan 77 days after the first imaging session to investigate retest variability of PET and arterial blood measurements.

Monkeys were transported from the BPRC to the VUmc in the morning, underwent PET scanning at approximately 11:00 and 14:00, and were returned to the research colony of the BPRC at the end of the afternoon. The animals were trained to voluntary enter their transit cages, and no anaesthesia was used during the 40-min transportation period. The animals were familiar with the procedures and personnel involved. At the PET-MRI facility, monkeys were sedated with an injection of the α2-adrenoceptor agonist medetomidine hydrochloride (60 µg/kg; Sedastart 1 mg/ml, AST Farma BV, Oudewater, the Netherlands) and midazolam (0.3 mg/kg; Midazolam Actavis 5 mg/ml; Actavis BV, Baarn, the Netherlands), which were administered intramuscularly. Two cephalic lines were placed, first for the induction and maintenance of propofol anaesthesia, which was delivered at a rate of 0.2 mg/kg/min (PropoVet Multidose 10 mg/ml, Fresenius Kabi AB, Uppsala, Sweden). The second line was placed to infuse NaCl/glucose for maintenance of fluid balance at a rate of 1 ml/kg/h (0.45 % sodium chloride & 2.5 % glucose 500 ml, Baxter BV, Utrecht, the Netherlands). Two arterial lines were placed in the femoral artery for continuous and discrete blood sampling. Xylocaine 10 % was used for endotracheal intubation to provide additional oxygen. The animals were allowed to breath freely during the anaesthesia. The monkeys were subsequently positioned in the scanner in the supine position, placed on a fluid heating system in order to maintain normothermia set at 38.5° (Small Animal Instruments Inc. [SAII], Stony Brook, NY, USA). SAII MR-compatible equipment was used to monitor haemoglobin oxygen saturation levels (SpO2), heart rate, and body temperature. Monitoring data were transmitted out the magnet bore by optical fibre cables to a control/gating module which resided in the MRI control room.

Radiprodil (UCB, Belgium) was used to block the GluN2B binding site of NMDA receptors. The drug was administered *via* the right cephalic vein 10 min prior to [11C]HACH242 injection at a dose of 10 mg/kg (free-baseweight) in a concentration of 5 mg/mL. The solution contained 2.5 % DMSO (dimethyl sulfoxide), 7.5 % Tween 80 (polysorbate) and sodium dihydrogen phosphate (NaH2PO4).

Radiopharmaceutical Preparation and Injectate

Radiosynthesis of N-((5-(4-fluoro-2-[11C]methoxyphenyl)pyridin-3-yl)methyl)cyclopentanamine ([11C]HACH242) was performed according to methods published previously [12]. Synthesis time including HPLC purification was approximately 90 min and radiochemical purity of the final product >98 %. The radiotracer was formulated in a phosphate-buffered saline solution containing 8.6 % ethanol, and administered by intravenous injection of ≤10 ml over a 10 s period.

Table 1. Subject and injectate details. A_m molar activity, *MBq* megabecquerel

	Age (years)	Weight (kg)	Injected activity scan 1 (MBq)	A_m PET1 (MBq·nmol^{-1})	Injected activity scan 2 (MBq)	A_m PET2 (MBq·nmol^{-1})
Subject 1	5.4	8.7	201	6.1	155	11.3
Subject 2	8.6	11.3	86	17.9	78	13.9
Subject 3	5.6	11.9	104	20.7	61	7.8
Subject 1 retest	5.7	8.7	113	23.6	72	22.7

Blood Sampling and Metabolite Analysis

Blood was withdrawn from the femoral arteries using an iRadimed MRidium 3850 infusion pump with a controlled withdrawal rate of 2.5 ml/min for a period of 6 min following [11C]HACH242 injection. Whole-blood radioactivity was measured with an on-line blood sampler detection system (Swisstrace twilight, Switzerland). In addition, discrete 3 ml blood samples were collected at set timepoints (5, 10, 20, 40, 60, 85 min postinjection [p.i.]) to measure plasma and whole-blood ratios, calibrate and extrapolate the whole-blood data, and determine metabolite fractions. Blood was collected into heparin tubes (Greiner Bio-One GmbH, Kremsmünster, Austria) and mixed by inversion. Plasma was separated from blood cells by centrifugation at 4000 rpm for 5 min at 4 °C using a Hettich Universal 16 table centrifuge (Hettich Benelux BV, Geldermalsen, the Netherlands). Activity concentrations of whole blood and plasma were measured in a gammacounter (Wizard 2480, Perkin Elmer). For metabolite analysis, 1 ml of plasma was diluted with 2 ml of water and passed over an activated tC18 Sep-Pak cartridge (Waters, the Netherlands). The Sep-Pak cartridge was washed with 5 ml of water. Recovered fractions were defined as the polar and non-polar radiolabelled metabolites. Thereafter, the tC18 Sep-Pak cartridge was eluted with 1.5 ml of methanol followed by 1.5 ml of water, and the fraction was further analysed by HPLC. The stationary phase consisted of a Phenomenex Gemini C18 5 µm 250 * 10 mm column (Phenomenex, Utrecht, the Netherlands). The mobile phase was A = acetonitrile B = H2O / 0,1 % ammonium acetate in a gradient system from 70 % B to 10 % B in 9 min at a flow of 3 ml/min. Fractions were collected and measured using a multiwell gammacounter (Wizard 2470, Perkin Elmer) and HPLC chromatograms were constructed.

Image Acquisition

The attenuation of the PET signal by tissues was derived from the MR data by performing a dedicated attenuation MR sequence. The scanner reconstruction software also accounts for the attenuation by the MR radiofrequency head coil using built-in template µ-map images. Ninety-minute dynamic PET data was acquired and binned into 38 time frames (1 × 10, 8 × 5, 4 × 10, 3 × 20, 5 × 30, 5 × 60, 4 × 150, 4 × 300, 2 × 600, 2 × 900 s). Reconstruction was performed using line-of-response row-action maximum likelihood algorithm (LOR-RAMLA). All data were normalised and corrected for scatter, random coincidences, attenuation, decay and dead time. Images were reconstructed into a matrix of 128 × 128 × 90 voxels, with an isotropic voxel size of 2 mm. Subject motion was checked by visual inspection of the alignment of intrasubject PET frames and no frames needed to be adjusted or excluded. T1-weighted MRI scans were co-registered to an average of the PET frames from ~ 0 to 2 min p.i. using VINCI software. Individual whole-brain masks were manually drawn on each subject's T1 MRI scan and on each averaged PET image (25–150 s frames) to guarantee coregistration to voxels in the brain only. Volumes of interest (VOIs) were defined using the INIA19 template for primate brain image parcellation [16] and applied as in previous PET studies [17]. VOIs included grey matter of the frontal, occipital and temporal cortex as well as the striatum (caudate and putamen) and cerebellum. Left and right hemisphere VOIs were combined for analysis. A grey-matter whole brain (global) VOI was defined separately. Time-activity curves (TAC) for each VOI were extracted from the dynamic PET scans using MATLAB® scripts (R2007b, The MathWorks, Natick, MA, USA) written in-house.

Statistical Analysis

Radioactivity concentration was expressed as counts per second per mm^3 of brain tissue (Bq/mm^3). Standardised uptake values (SUV, equaling measured activity divided by injected dose per body weight) were calculated from measured radioactivity in each VOI. The area under the curve (AUC) of [11C]HACH242 brain uptake (0–82.5 min; frame midpoint times) and arterial parent fraction in plasma were estimated by means of the trapezoidal algorithm for each scan. The SUV coefficient of variation between-subjects (CV) was computed by dividing the SUV standard deviation (SD) by the mean. Plasma SUV at each time point was calculated as well as the AUC. Finally, the plasma parent fraction was multiplied by the corresponding plasma SUV at each time point. Reliable input functions for kinetic modelling could not be generated because of variability in the whole blood radioactivity measurement during the first minutes after tracer injection. The brain to plasma partition coefficient, that is, the ratio of [11C]HACH242 concentration in brain to that in plasma (K_P), was obtained by calculating the ratio between brain SUV_{AUC} to the individual parent $plasma_{AUC}$. Results are presented as mean ± standard deviation (SD).

Results

[11C]HACH242 readily entered the brain and displayed a fairly uniform pattern of uptake (Fig. 2). Individual subject SUVs at baseline and after radiprodil administration are shown in Fig. 3 and summarised in Table 2. The peak uptake in whole brain grey matter during radiprodil scans was increased by 20 % in subject 1 but reduced by 9 %, 1 % and 20 % for subjects 2, 3 and the retest of subject 1, respectively, compared to baseline. SUV in the last 15-min PET frame was 17 to 25 % higher in the radiprodil condition for subject 1, but approximately equal (1 to 3 %) in subjects 2 and 3. Covariance of SUV_{AUC} between subjects for the four baseline scans was 12 %. The SUV of [11C]HACH242 in whole brain, frontal cortex and cerebellum grey matter when normalised for individual peak uptake are shown in

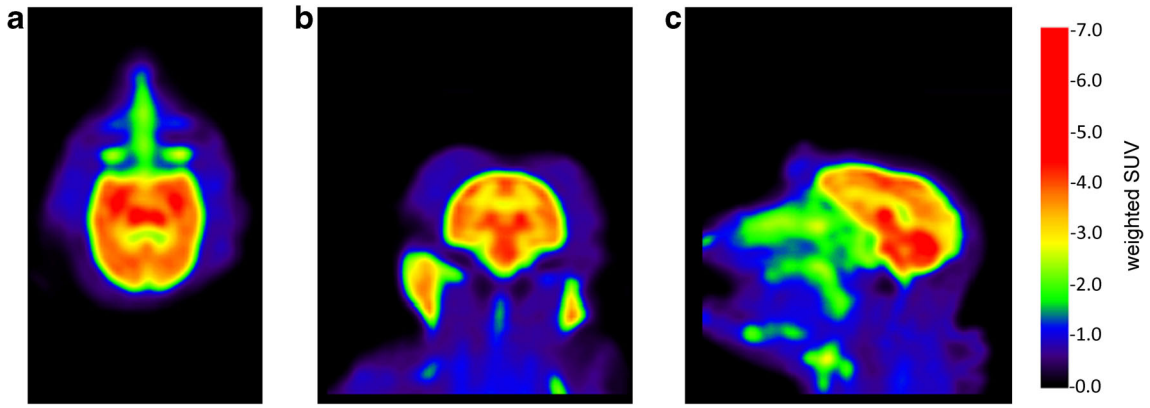

Fig. 2. **a** Transaxial, **b** coronal and **c** sagittal views of time-weighted SUV PET images from 0 to 90 min.

Fig. 3b. Slower washout in the radiprodil condition resulted in slight SUV increases in the last PET frame compared with peak uptake of 4 to 11 % for subjects 1, 2 and 3 and 45 % for the retest of subject 1.

Plasma Analysis

Radioactivity measurements in blood and plasma, as well as tracer metabolism are shown in Fig. 4. Blood could not be sampled from the artery during the radiprodil scan of subject 3, therefore results of four baseline scans and three radiprodil scans are reported. Mean parent fraction in all seven scans was 52 ± 16 % at 5 min, 35 ± 13 % at 10 min, 26 % ± 10 at 20 min, 15 ± 4 % at 40 min, 13 ± 6 % at 60 min, and 8 ± 5 % at 85 min p.i. HPLC analysis demonstrated that the polar fraction and 1 major metabolite accounted for the remaining radioactivity (Fig. 4b). Polar metabolites constituted 52 ± 10 % at 10 min and 76 ± 8 % at 85 min p.i. The mean nonpolar metabolite fraction was approximately 9 % from 10 min p.i. until the end of the scan (not displayed). Mean AUC of [11C]HACH242 parent fraction for baseline scans was 1316 (range 733–2025) and for radipril scans 1689 (range 1170–2026). Total plasma SUV_{AUC} was reduced by 11 %, 45 and 56 % in the radiprodil scans compared to baseline.

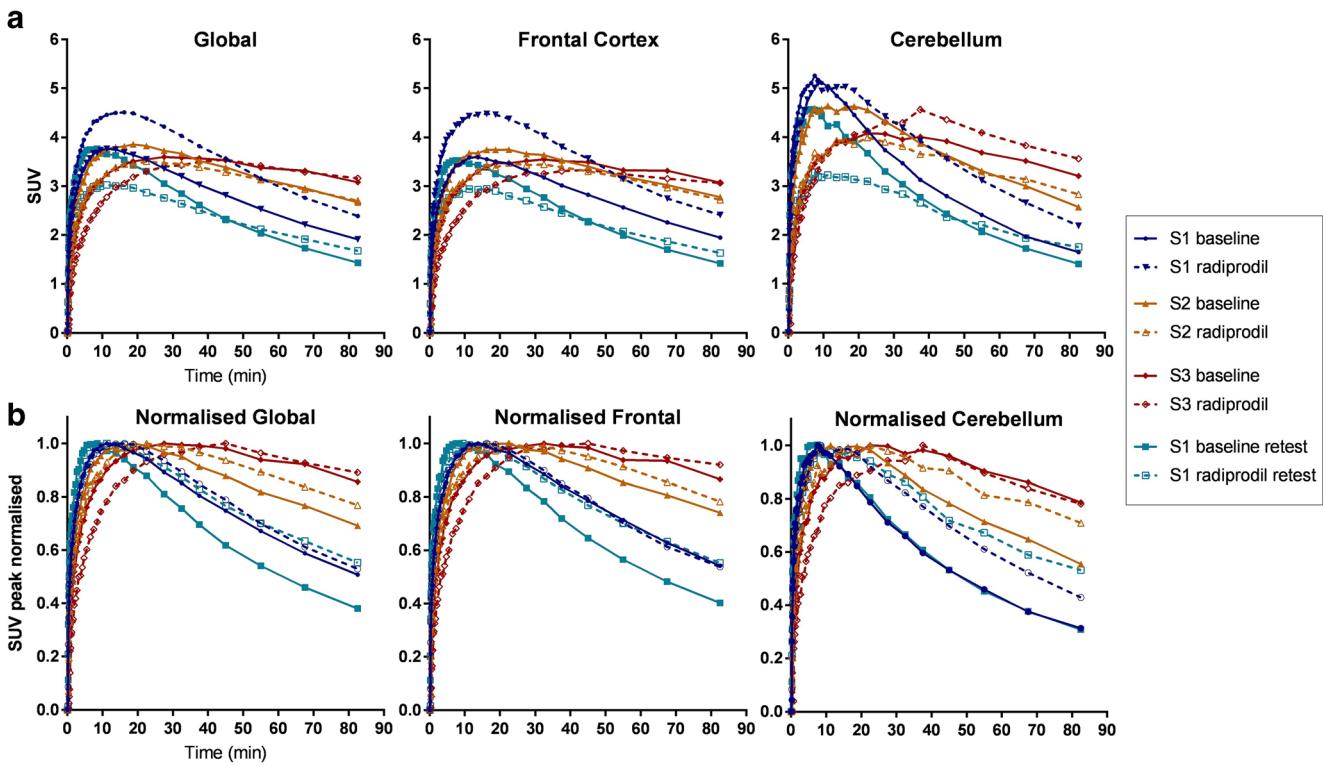

Fig. 3. **a** Individual subject SUVs for whole-brain grey matter (global), frontal cortex and cerebellum and **b** normalised for peak uptake.

Table 2. [11C]HACH242 standardised uptake values (SUV) and areas under the curve (AUC) of brain and plasma parent fraction per subject and treatment

		Subject 1	Subject 2	Subject 3	Subject 1 Retest	Mean	SD	S1 test-retest change
SUV_{Peak}	Baseline	3.77	3.86	3.60	3.76	3.75	0.11	0 %
	Radiprodil	4.51	3.51	3.55	3.03	3.65	0.62	−33 %
	Change	20 %	−9 %	−1 %	−20 %	−3 %	17 %	
$SUV_{75–90\ min}$	Baseline	1.91	2.67	3.08	1.43	2.27	0.74	−25 %
	Radiprodil	2.39	2.70	3.16	1.68	2.48	0.62	−30 %
	Change	25 %	1 %	3 %	17 %	11 %	12 %	
$SUV_{75–90\ min}$ divided by SUV_{Peak}	Baseline	0.51	0.69	0.86	0.38	0.61	0.21	−25 %
	Radiprodil	0.53	0.77	0.89	0.55	0.69	0.17	5 %
	Change	4 %	11 %	4 %	45 %	16 %	20 %	
$Plasma_{AUC}$ parent fraction	Baseline	44.3	56.2	30.9	79.9	52.8	20.8	80 %
	Radiprodil	39.5	30.9		35.5	35.3	4.29	−10 %
	Change	−11 %	−45 %		−56 %	−37 %	23 %	
SUV_{AUC} normalised for $Plasma_{AUC}$	Baseline	5.32	4.83	8.79	2.62	5.39	2.55	−51 %
	Radiprodil	7.37	8.28		5.52	7.06	1.41	−25 %
	Change	39 %	72 %		110 %	74 %	36 %	

SUV_{AUC} of [11C]HACH242 in the brain divided by the $plasma_{AUC}$ was 39 %, 72 and 110 % higher in the radiprodil condition for subjects 1, 2 and subject 1 retest, respectively. This change was partly driven by lower $plasma_{AUC}$ in the radiprodil scans (−11 %, −45 % and − 56 % respectively). Radiprodil administration did not affect the change in [11C]HACH242 brain-to-plasma ratio differently in the brain VOIs when compared to baseline brain-to-plasma ratios.

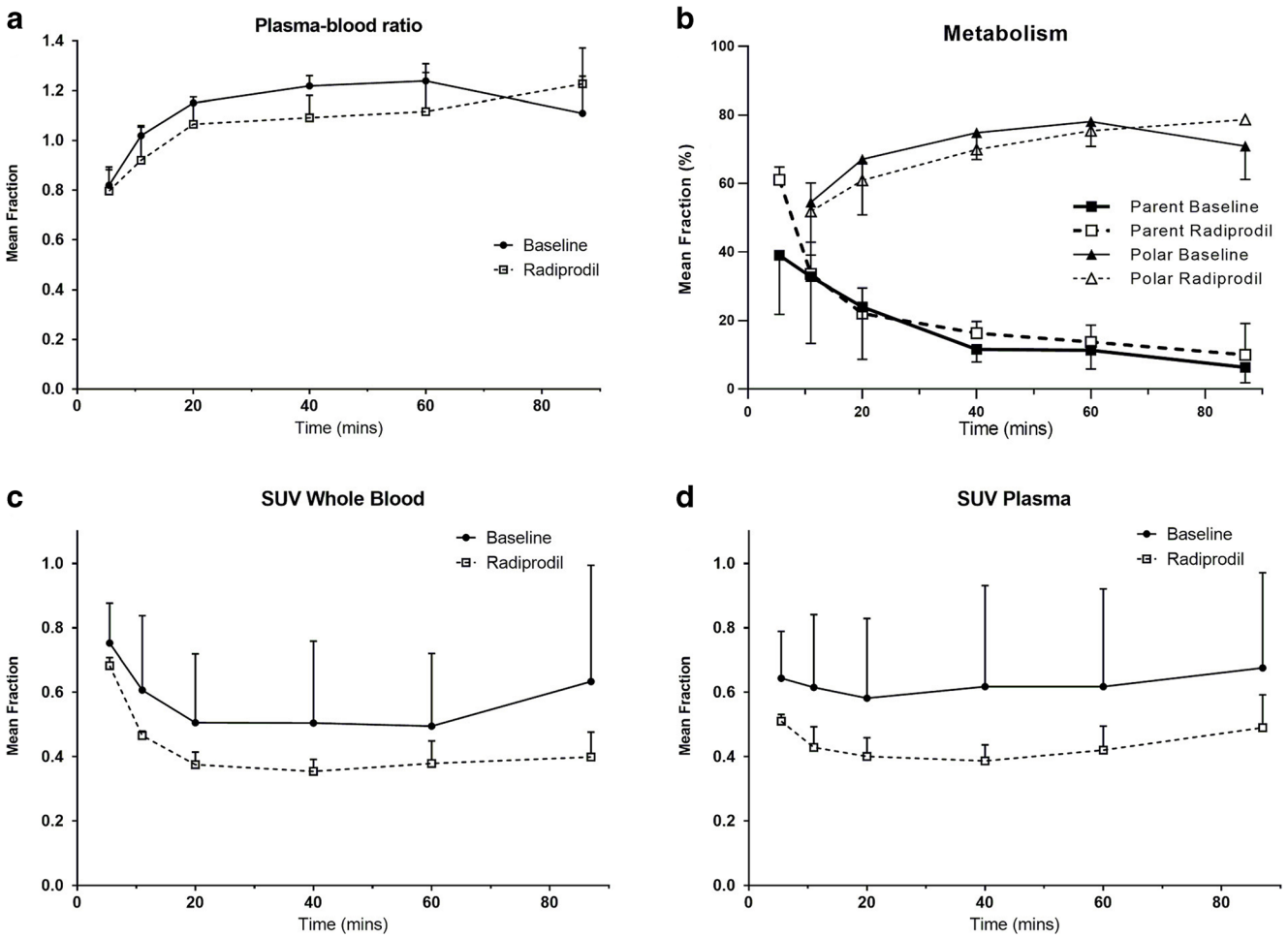

Fig. 4. **a** Plasma-to-blood ratio, **b** the mean percentage of plasma radioactivity attributable to parent [11C]HACH242 and polar metabolites, **c** the standardised uptake value (SUV) of whole blood radioactivity and **d** SUV of plasma radioactivity multiplied by the parent fraction. Results at each time-point are presented as the mean ± SD fractions from baseline ($N = 4$) and radiprodil ($N = 3$) scans.

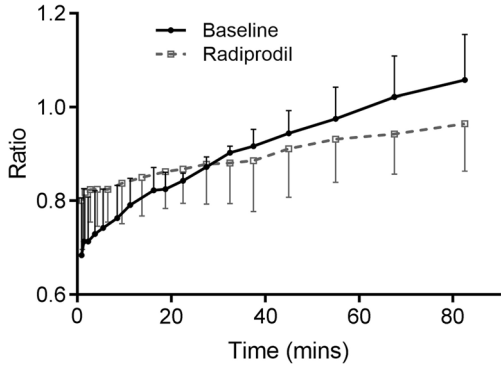

Fig. 5. Mean SUV ratio (SUVR) of the frontal cortex over cerebellum of all 4 baseline and radiprodil scans. Error bars represent standard deviations.

Figure 5 shows that the average [^{11}C]HACH242 uptake in the frontal cortex at baseline condition was initially 68 % of cerebellum uptake (range 52–83 %), and increased to 106 % (range 96–118 %) at the end of the scan. After radiprodil administration, the average SUV in the frontal cortex is more in line with the cerebellum SUV, starting at 80 % (range 68–93 %) and reaching 96 % (range 86–110 %) of the cerebellum uptake at the end of the scan.

Discussion

This study describes the first *in vivo* evaluation of the radiotracer [^{11}C]HACH242 in the primate brain. [^{11}C]HACH242 TACs in the brain showed appropriate reversible pharmacokinetics within the timeframe of the PET scan. Systemic plasma clearance of the parent compound remained constant throughout the scan and was lower than clearance from brain VOIs. No consistent reduction was observed in [^{11}C]HACH242 SUVs after intravenous infusion of radiprodil, a GluN2B negative allosteric modulator. Radiprodil distribution studies in rodents showed that it has unrestricted access to the brain tissue with brain-to-plasma ratios of ~1 and a terminal half-life of 3.2 h in dogs (UCB Pharma, unpublished communication). Radiprodil was therefore expected to decrease the SUV ratio at late time frames in VOIs with high *vs* low GluN2B binding sites. This could be suggestive of lower specific binding of [^{11}C]HACH242, under the assumption that the radiotracer kinetics in plasma are equal in both conditions. The main limitation of this study is that reliable input functions for kinetic modelling could not be generated because of variability in the whole blood radioactivity measurement during the first minutes after tracer injection. However, interpretation of the [^{11}C]HACH242 kinetics in different brain VOIs in relation to plasma metabolism and clearance allows for deductions to be made about the underlying physiological processes.

In previous studies in mice, [^{11}C]HACH242 showed high specific binding and heterogeneous distribution in brain slices that was similar to the expression of NMDA receptors. For example, a threefold increase in activity uptake was measured in forebrain regions *vs.* cerebellum at 15 min [9]. Results in the present study show that average [^{11}C]HACH242 peak uptake in the frontal cortex at baseline condition is 30 % lower than cerebellum uptake and 10 % higher at the end of the scan. This suggests a lower perfusion of the tracer into the frontal cortex and a somewhat slower washout. After radiprodil administration, the uptake in the cerebellum is more in line with the frontal cortex (Fig. 5). The lower ratio from 30 min to the end of the scan could suggest that binding of [^{11}C]HACH242 to GluN2B in the frontal cortex is reduced relative to cerebellum binding. However, the ratio change can be explained largely by the change in the cerebellar TACs after radiprodil administration. In another effort to compare the effect of radiprodil on [^{11}C]HACH242 binding, SUVs were normalised to the individual peak uptake (Fig. 3b). GluN2B saturation was expected to accelerate the washoff and reveal the degree of specific binding. However, slower washout in the radiprodil condition was observed, resulting in SUV increases in the last PET frame of 4 to 11 % for subjects 1 to 3 and 45 % for the retest of subject 1. The baseline TACs of the cerebellum were similar for subject 1 test and retest scans after normalisation to peak uptake, indicating good TAC test-retest reproducibility in a VOI with relatively low density of the target. *In situ* hybridisation studies of GluN2B have shown that mRNA expression patterns of the GluN2B subunit are similar between humans, monkeys, and mice in most brain regions [18]. The NR2B subunit is found predominantly in hippocampus, cerebral cortex, striatum and olfactory bulbs, as shown by immuno-cytochemical localisation studies [19]. The present baseline PET data indicate slower washout in cortex than in cerebellum, as could be expected based on the target density. Although *in vitro* autoradiography of [^{11}C]HACH242 in the brain of rhesus monkey has not been performed yet, the widespread distribution of GluN2B suggests that a reference region in the brain devoid of GluN2B binding sites is not available, which prevented the exploration of reference tissue compartmental models to fit to the PET data. An additional complexity in the interpretation of the current results is the affinity of [^{11}C]HACH242 to sigma-1 receptors (20 nM) in the brain. A postmortem human brain study found moderate levels of sigma-1 receptor mRNA distributed in the cortex, with the temporal cortex being particularly enriched [20]. Although experiments to confirm the affinity of [^{11}C]HACH242 to sigma-1 in primates are warranted, it is reasonable to assume that the measured [^{11}C]HACH242 PET signal constitutes binding to both GluN2B and sigma-1, which could confound interpretation of (clinical) data. The degree of specific binding to GluN2B in mice was shown to vary between 3 and 40 % [12]. Dense labelling was observed in brain regions that do not express high levels of GluN2B subunit-containing NMDA receptors, suggesting binding to sigma-1 or other proteins. Future research could employ a sigma-1 receptor compound such as the agonist fluvoxamine in combination with a GluN2B negative

allosteric modulator to assess the binding potential of [11C]HACH242. Importantly, however, a recent PET study in rats showed that the sigma-1 receptor agonist (1)-pentazocine abolished [11C]Me-NB1-specific binding in the brain, despite the lack of direct competition *in vitro* and a 33-fold selectivity of [11C]Me-NB1 for the human GluN2B receptor over sigma 1 [21]. It was hypothesised that an interaction between sigma-1 agonism and GluN2B in the living brain could hamper binding of [11C]Me-NB1, which is structurally comparable with [11C]HACH242. It would be valuable to further investigate [11C]HACH242 kinetics following administration of a sigma-1 agonist to confirm the findings of an *in vivo* PET signal block.

The change in [11C]HACH242 brain uptake and washout following radiprodil administration may be a consequence of the drug's effect on the delivery of parent [11C]HACH242 from blood to tissue. Results showed that SUV in blood and plasma, as well as the plasma-to-blood ratio were reduced in the radiprodil condition compared to baseline. A lower AUC of plasma parent fraction was also observed in the three radiprodil scans for which data was available (−11 %, −45 % and − 56 % compared to baseline). Binding in peripheral sites or to plasma proteins might have been altered by radiprodil, resulting in a different pattern of uptake in the brain. However, a closer look at the individual TACs does not show a clear relationship between SUV_{AUC} in plasma and brain. Fast peripheral metabolism of [11C]HACH242 and rapid clearance of the parent tracer from plasma hindered prolonged measurements of [11C]HACH242 from arterial plasma. Errors in the estimation of arterial blood parameters are probable. For example, the whole-blood activity at 85 min in the radiprodil retest scan of subject 1 was 40 % higher than the previous samples resulting in aberrant group averages (Fig. 4). Polar metabolites made up 50 % of measured radioactivity in plasma at 10 min p.i., compared with 75 % in previous *in vivo* [11C]HACH242 experiments in mice [6]. In general, it is assumed that polar metabolites do not cross the blood-brain barrier, but even if they do, they will only increase the non-specific signal. The non-polar metabolite fraction remained less than 10 % throughout the time of the scan. Therefore, even if these lipophilic metabolites cross the blood-brain barrier, they would constitute only a minor fraction of total cerebral uptake. Nevertheless, future studies are needed to assess the behaviour of the labelled metabolites in the brain.

It is possible that changes in cerebral blood flow (CBF) contributed to the difference between baseline and radiprodil [11C]HACH242 SUV. There are currently no scientific reports available that have investigated with PET or MRI the effect of "prodils" or other GluN2B negative allosteric modulators on CBF in the healthy brain. One study on the protective effects of ifenprodil on ischemia used laser doppler flowmetry and showed that there was no significant change in cerebral blood flow [22]. In the present study, the anaesthestics medetomidine and midazolam were administered intramuscularly approximately 2 h before the baseline PET scan, equating to ~6 h before the radiprodil scan. Considering medetomidine's time to peak concentration and half-life of ~30 min following i.m. administration [23], the plasma and brain concentrations may still have been high enough to exert pharmacodynamic effects in the baseline scan. Reports of the effect of anaesthesia on CBF are important in this regard. A SPECT study in dogs showed that medetomidine increased the regional CBF in all brain regions bar the subcortical (thalamic) area [24]. Consistent with increased CBF, [11C]HACH242 TACs showed higher uptake and faster washout in the baseline scan. However, midazolam, which was co-administered with medetomidine, has been shown to reduce global CBF dose-dependently in humans [25]. Propofol was injected intravenously at a constant rate during the entire scan day for maintenance of anaesthesia and therefore should not have affected CBF differently between the two [11C]HACH242 PET scans on the same day. Polypharmacological effects, which potentially modulate multiple targets in the brain, complicate predictions of regional CBF effects. Ketamine is commonly used as a sole anaesthetic agent in NHP studies. However, this compound acts on the NMDA receptor [26] and, therefore, it was not suitable for implementation in the current study. Opioidergic compounds such as fentanyl can affect NMDA receptor function [17], and hence propofol was deemed the most appropriate anaesthetic in the present study design. Future attempts at visualising the GluN2B binding site of the NMDA receptor are preferably performed in awake primates or humans to exclude potential CBF effects of anaesthetics. Simultaneous [11C]HACH242 PET and fMRI could elucidate the relationship between NMDA receptor blockers, blood flow and radiotracer binding [27].

Preclinical experiments with [11C]HACH242 have shown that anaesthesia in mice, administered as a mixture of fentanyl, fluanisone and midazolam, resulted in inconsistent effects on brain uptake of [11C]HACH242 following pretreatment with Ro25-6981 [6]. Specifically, Ro25-6981 induced either a mean 22 % decrease or a mean 29 % increase in radioactivity uptake across all brain regions analysed in *ex vivo* brains 20 min after radiotracer injection. It is striking that in the present study there was considerable test-retest variability of subject 1 SUV in brain and plasma. PET experiments performed in NHP under awake conditions with the C-11 labelled analogue of the GluN2B-selective ligand CP-101,606 showed no appreciable specific binding [28]. Endogenous ligands of the NMDA receptor such as spermine and spermidine, as well as divalent cations, strongly inhibited radiolabelled CP-101,606 binding in the order of $Zn^{2+} > Mg^{2+} > Ca^{2+}$ at their physiological concentrations. L-glutamate and NMDA tended to slightly increase the binding, while glycine and D-serine showed no effect [28]. Discrepancies between *in vitro* and *in vivo* binding properties of radiotracers developed for the GluN2B binding site have been reported for other NMDA receptor radiotracers [21, 29]. Ifenprodil and spermine inhibited the *in vitro* binding of C-11 labelled bis(phenylalkyl)amines

with potencies similar to those of non-radioactive ligand. However, *in vivo* pre-treatment with non-radioactive tracer caused an increase of binding in the cerebral cortex and hippocampus compared with the control group [29]. Estimating the [11C]HACH242 binding potential *in vivo* is complicated by the atypical mode of action of GluN2B-containing NMDA receptors. For example, binding is context-dependent [30], such that strongly activated receptors are preferentially inhibited. In addition, GluN2B-selective antagonists can divide into two distinct classes according to binding pose, resulting in strikingly different ligand orientation and receptor interactions [31]. Taken together, there are various receptor interactions and biophysical factors that affect *in vivo* binding properties of NMDA receptor radioligands, which remain to be tested, for example using bolus-plus-infusion PET experiments in awake primates while monitoring hemodynamic changes [27].

Conclusions

The present results show that [11C]HACH242 has a suitable kinetic profile in the brain and low accumulation of lipophilic radiometabolites. Under the tested conditions, however, the specific binding of [11C]HACH242 *in vivo* using PET could not be visualised. The divergent preclinical behaviour in mice and primates could be a consequence of variations in cerebral blood flow, a low fraction of specifically bound tracer, or interactions of the radiotracer with the sigma-1 receptor or endogenous ligands at the binding site. The typical study design for neuroreceptor PET tracers executed here may not be applicable to such a dynamic and complex receptor system as the GluN2B site of the NMDA receptor. Further experiments of ligand interactions are necessary in order to facilitate the development of radiotracers for *in vivo* imaging of the ionotropic NMDA receptor.

Acknowledgements. We thank the PET-MRI technicians for their support with the execution of the study.

Funding. This study was funded by the framework of CTMM, the Center for Translational Molecular Medicine (www.ctmm.nl), project LeARN (grant 02N-101).

Compliance with Ethical Standards

Conflict of Interest

The authors declare that they have no conflict of interest.

References

1. Paoletti P, Bellone C, Zhou Q (2013) NMDA receptor subunit diversity: impact on receptor properties, synaptic plasticity and disease. Nat Rev Neurosci 14:383–400
2. Mony L, Krzaczkowski L, Leonetti M, le Goff A, Alarcon K, Neyton J, Bertrand HO, Acher F, Paoletti P (2009) Structural basis of NR2B-selective antagonist recognition by N-methyl-D-aspartate receptors. Mol Pharmacol 75:60–74
3. Loftis JM, Janowsky A (2003) The N-methyl-d-aspartate receptor subunit NR2B: localization, functional properties, regulation, and clinical implications. Pharmacol Ther 97:55–85
4. Laurie DJ, Bartke I, Schoepfer R, Naujoks K, Seeburg PH (1997) Regional, developmental and interspecies expression of the four NMDAR2 subunits, examined using monoclonal antibodies. Brain Res Mol Brain Res 51:23–32
5. Sobrio F, Gilbert G, Perrio C, Barre L, Debruyne D (2010) PET and SPECT imaging of the NMDA receptor system: an overview of radiotracer development. Mini Rev Med Chem 10:870–886
6. Klein PJ, Christiaans JAM, Metaxas A, Schuit RC, Lammertsma AA, van Berckel BNM, Windhorst AD (2015) Synthesis, structure activity relationship, radiolabeling and preclinical evaluation of high affinity ligands for the ion channel of the N-methyl-d-aspartate receptor as potential imaging probes for positron emission tomography. Bioorg Med Chem 23:1189–1206
7. Fuchigami T, Nakayama M, Yoshida S (2015) Development of PET and SPECT probes for glutamate receptors. Sci World J 2015:1–19
8. Labas R, Gilbert G, Nicole O, Dhilly M, Abbas A, Tirel O, Buisson A, Henry J, Barré L, Debruyne D, Sobrio F (2011) Synthesis, evaluation and metabolic studies of radiotracers containing a 4-(4-[18F]-fluorobenzyl)piperidin-1-yl moiety for the PET imaging of NR2B NMDA receptors. Eur J Med Chem 46:2295–2309
9. van der Aart J, Golla SSV, van der Pluijm M, Schwarte LA, Schuit RC, Klein PJ, Metaxas A, Windhorst AD, Boellaard R, Lammertsma AA, van Berckel BNM (2018) First in human evaluation of [18F]PK-209, a PET ligand for the ion channel binding site of NMDA receptors. EJNMMI Res Res 8:69
10. Roger G, Dollé F, De Bruin B, Liu X, Besret L, Bramoullé Y, Coulon C, Ottaviani M, Bottlaender M, Valette H, Kassiou M (2004) Radiosynthesis and pharmacological evaluation of [11C]EMD-95885: a high affinity ligand for NR2B-containing NMDA receptors. Bioorg Med Chem 12:3229–3237
11. Brown DG, Maier DL, Sylvester MA, Hoerter TN, Menhaji-Klotz E, Lasota CC, Hirata LT, Wilkins DE, Scott CW, Trivedi S, Chen T, McCarthy DJ, Maciag CM, Sutton EJ, Cumberledge J, Mathisen D, Roberts J, Gupta A, Liu F, Elmore CS, Alhambra C, Krumrine JR, Wang X, Ciaccio PJ, Wood MW, Campbell JB, Johansson MJ, Xia J, Wen X, Jiang J, Wang X, Peng Z, Hu T, Wang J (2011) 2,6-Disubstituted pyrazines and related analogs as NR2B site antagonists of the NMDA receptor with anti-depressant activity. Bioorg Med Chem Lett 21:3399–3403
12. Christiaans JAM, Klein PJ, Metaxas A, Kooijman EJM, Schuit RC, Leysen JE, Lammertsma AA, van Berckel BNM, Windhorst AD (2014) Synthesis and preclinical evaluation of carbon-11 labelled N-((5-(4-fluoro-2-[11C]methoxyphenyl)pyridin-3-yl)methyl)cyclopentanamine as a PET tracer for NR2B subunit-containing NMDA receptors. Nucl Med Biol 41:670–680
13. Toyohara J, Sakata M, Ishiwata K (2012) Re-evaluation of in vivo selectivity of [11C]SA4503 to σ(1) receptors in the brain: contributions of emopamil binding protein. Nucl Med Biol 39:1049–1052
14. Bradford AM (2006) Molecular pharmacology of a novel NR2B-selective NMDA receptor antagonist. Doctoral thesis. In: Durham University
15. Weatherall D, Goodfellow P, Harris J, Hinde R, Johnson L, Morris R, Ross N, Skehel J, Tickell C (2006) The use of non-human primates in research. The Royal Society, London
16. Rohlfing T, Kroenke CD, Sullivan EV, Dubach MF, Bowden DM, Grant KA, Pfefferbaum A (2012) The INIA19 template and NeuroMaps atlas for primate brain image parcellation and spatial normalization. Front Neuroinform 6:27
17. Golla SSV, Klein PJ, Bakker J, Schuit RC, Christiaans JAM, van Geest L, Kooijman EJM, Oropeza-Seguias GM, Langermans JAM, Leysen JE, Boellaard R, Windhorst AD, van Berckel BNM, Metaxas

A (2015) Preclinical evaluation of [^{18}F]PK-209, a new PET ligand for imaging the ion-channel site of NMDA receptors. Nucl Med Biol 42:205–212
18. Bai L, Hof PR, Standaert DG, Xing Y, Nelson SE, Young AB, Magnusson KR (2004) Changes in the expression of the NR2B subunit during aging in macaque monkeys. Neurobiol Aging 25:201–208
19. Charton JP, Herkert M, Becker CM, Schröder H (1999) Cellular and subcellular localization of the 2B-subunit of the NMDA receptor in the adult rat telencephalon. Brain Res 816:609–617
20. Kitaichi K, Chabot JG, Moebius FF, Flandorfer A, Glossmann H, Quirion R (2000) Expression of the purported sigma(1) receptor in the mammalian brain and its possible relevance in deficits induced by antagonism of the NMDA receptor complex as revealed using an antisense strategy. J Chem Neuroanat 20:375–387
21. Krämer SD, Betzel T, Mu L, Haider A, Herde AM, Boninsegni AK, Keller C, Szermerski M, Schibli R, Wünsch B, Ametamey SM (2018) Evaluation of [^{11}C]Me-NB1 as a potential PET radioligand for measuring GluN2B-containing NMDA receptors, drug occupancy and receptor crosstalk. J Nucl Med 59:698–703
22. Başkaya MK, Rao AM, Donaldson D, Prasad MR, Dempsey RJ (1997) Protective effects of ifenprodil on ischemic injury size, blood-brain barrier breakdown, and edema formation in focal cerebral ischemia. Neurosurgery 40:364–370
23. Kastner SBR, Wapf P, Feige K, Demuth D, Bettschart- Wolfensberger R, Akens MK, Huhtinen M (2003) Pharmacokinetics and sedative effects of intramuscular medetomidine in domestic sheep. J Vet Pharmacol Ther 26:271–276
24. Waelbers T, Peremans K, Vermeire S, Duchateau L, Dobbeleir A, Audenaert K, Polis I (2011) The effect of medetomidine on the regional cerebral blood flow in dogs measured using technetium-99m-ethyl cysteinate dimer SPECT. Res Vet Sci 91:138–143
25. Veselis RA, Reinsel RA, Beattie BJ, Mawlawi OR, Feshchenko VA, DiResta GR, Larson SM, Blasberg RG (1997) Midazolam changes cerebral blood flow in discrete brain regions: an $H_2{}^{15}O$ positron emission tomography study. Anesthesiology 87:1106–1117
26. van der Doef TF, Golla SSV, Klein PJ, Oropeza-Seguias GM, Schuit RC, Metaxas A, Jobse E, Schwarte LA, Windhorst AD, Lammertsma AA, van Berckel BNM, Boellaard R (2016) Quantification of the novel N-methyl-d-aspartate receptor ligand [^{11}C]GMOM in man. J Cereb Blood Flow Metab 36:1111–1121
27. Schoenberger M, Schroeder FA, Placzek MS, Carter RL, Rosen BR, Hooker JM, Sander CY (2018) In vivo [^{18}F]GE-179 brain signal does not show NMDA-specific modulation with drug challenges in rodents and nonhuman primates. ACS Chem Neurosci 9:298–305
28. Haradahira T, Maeda J, Okauchi T, Zhang MR, Hojo J, Kida T, Arai T, Yamamoto F, Sasaki S, Maeda M, Suzuki K, Suhara T (2002) Synthesis, in vitro and in vivo pharmacology of a C-11 labeled analog of CP-101,606, (+/−)threo-1-(4-hydroxyphenyl)-2-[4-hydroxy-4-(p-[^{11}C]methoxyphenyl)piperidino]-1-propanol, as a PET tracer for NR2B subunit-containing NMDA receptors. Nucl Med Biol 29:517–525
29. Sasaki S, Kurosaki F, Haradahira T, Yamamoto F, Maeda J, Okauchi T, Suzuki K, Suhara T, Maeda M (2004) Synthesis of ^{11}C-labelled bis(phenylalkyl)amines and their in vitro and in vivo binding properties in rodent and monkey brains. Biol Pharm Bull 27:531–537
30. Yuan H, Myers SJ, Wells G, Nicholson KL, Swanger SA, Lyuboslavsky P, Tahirovic YA, Menaldino DS, Ganesh T, Wilson LJ, Liotta DC, Snyder JP, Traynelis SF (2015) Context-dependent GluN2B-selective inhibitors of NMDA receptor function are neuroprotective with minimal side effects. Neuron 85:1305–1318
31. Stroebel D, Buhl DL, Knafels JD, Chanda PK, Green M, Sciabola S, Mony L, Paoletti P, Pandit J (2016) A novel binding mode reveals two distinct classes of NMDA receptor GluN2B-selective antagonists. Mol Pharmacol 89:541–551